



**HAL**  
open science

# Entropy generation minimization in a channel flow: Application to different advection-diffusion processes and boundary conditions

J.M. Avellaneda, F. Bataille, A. Toutant, G. Flamant, M.A. Keilany, M.  
Milhé, J-J. Bézian, Q. Falcoz

## ► To cite this version:

J.M. Avellaneda, F. Bataille, A. Toutant, G. Flamant, M.A. Keilany, et al.. Entropy generation minimization in a channel flow: Application to different advection-diffusion processes and boundary conditions. *Chemical Engineering Science*, 2020, 220, pp.115601. 10.1016/j.ces.2020.115601 . hal-03523216

**HAL Id: hal-03523216**

**<https://univ-perp.hal.science/hal-03523216>**

Submitted on 20 May 2022

**HAL** is a multi-disciplinary open access archive for the deposit and dissemination of scientific research documents, whether they are published or not. The documents may come from teaching and research institutions in France or abroad, or from public or private research centers.

L'archive ouverte pluridisciplinaire **HAL**, est destinée au dépôt et à la diffusion de documents scientifiques de niveau recherche, publiés ou non, émanant des établissements d'enseignement et de recherche français ou étrangers, des laboratoires publics ou privés.



Distributed under a Creative Commons Attribution - NonCommercial 4.0 International License

# Entropy generation minimization in a channel flow: application to different advection-diffusion processes and boundary conditions

J.M. Avellaneda<sup>a,\*</sup>, F. Bataille<sup>a</sup>, A. Toutant<sup>a</sup>, G. Flamant<sup>b</sup>

<sup>a</sup>PROMES-CNRS, UPR 8521, University of Perpignan Via Domitia, 66100 Perpignan, France

<sup>b</sup>PROMES-CNRS, UPR 8521, 7 rue du Four solaire, 66120 Font Romeu, France

## Abstract

Heat and mass transfer enhancement in a convective flow is studied using a variational optimization technique. Entropy generation rate is minimized while allowing to vary the relative weight of the total viscous dissipation in the objective functional to determine optimized velocity and scalar field patterns. The resulting velocity, thermal and mass concentration fields are analyzed as well as the influence of boundary conditions. The relative improvement of the optimized solutions is assessed and heat transfer vs. mass diffusion results are compared. The optimization approach leads to improved entropy generation rates. The viscous dissipation weighting factor influences the entropy generation rates and the velocity and scalar field patterns. A transition between two levels of perturbation by comparison to non-optimized flows occurs at a critical value of the weighting factor that depends on the boundary conditions. The flow patterns obtained by variational optimization can be the basis for enhanced exchanger design.

**Keywords:** Second law, Heat and mass transfer, Optimization, Variational analysis, Entropy minimization

## 1. Introduction

This study addresses the application of variational methods to improve heat and mass transfers in convective flows with optimal velocity fields as a result. In many industries and engineering applications, it is necessary to optimize heat or mass transfers in order to improve the technical or economic efficiency of machines, plants or processes. The intensification of heat transfer is sought in thermal power plants like concentrated solar [1, 2, 3, 4], nuclear [5] or geothermal [6] ones, but also in the process, automotive or aerospace industries and for cooling systems. Heat transfer enhancement is an innovative field of research [7] that uses many techniques whether active (requiring an external energy input) such as the use of oscillating walls, or passive such as the addition of mixing promoters in the flow channel [8] [9] or the search for optimized transfer fluids. Convective mass transfer enhancement is also an area of particular interest for chemical processes [10] and biotechnology [11, 12] that take advantage of passive [13, 14] or active methods [15, 16]. In both heat transfer and mass diffu-

sion, the use of suspended fine particles [17] or nanofluids [18, 19] is also being studied to increase exchanges. The intensification of heat or mass transfers is often produced by the passive promotion or the active realization of mixing [20] whose performance is dependent on the fluid flow pattern [21, 22, 23]. Therefore, searching for optimal flow patterns can be useful to improve heat or mass transfer in convective flows.

One way to address this issue is applying thermodynamic optimization by using the entropy generation rate as a criterion [24, 25]. In convective flow heat and mass transfer, the total entropy generation rate is generally a sum of several terms. In the absence of radiative heat transfer [26], chemical reaction [27, 28], cross effects such as Dufour or Soret ones [29] and dissipation related to electric or magnetic fields [30, 31], the entropy generation rate originates from viscous friction, on the one hand, and from the diffusion of heat or mass through finite temperature or mass concentration differences, on the other hand. Acting on one of the two terms, for example by reducing the rate of heat conduction entropy generation, can lead to an increase in viscous friction entropy generation and it is necessary to seek the right compromise between two opposing effects. The total generated entropy rate can be minimized in order to find this optimal trade-off [32, 33, 34]. It is also possible to

\*Corresponding author

Email address: [jean-marc.avellaneda@promes.cnrs.fr](mailto:jean-marc.avellaneda@promes.cnrs.fr)  
(J.M. Avellaneda)

look for a minimum of entropy generation while fixing a constraint on the total viscous dissipation in the flow [35, 36], the latter being related to the pressure drop, which is a quantity to be controlled in industrial applications.

In the present study, the calculus of variations is used to minimize a functional objective constructed as a linear combination of the entropy generation rate main contributor on the one hand and the viscous dissipation on the other hand [37, 38, 39, 40]. A weighting coefficient allowing to give more or less importance to the viscous dissipation during the optimization process is used. For each value of this weighting factor, the optimal velocity and scalar fields are obtained by varying a volume force field source term and the resulting improvement in entropy generation rate is calculated. The method is applied to heat transfer and mass diffusion cases in order to identify common behaviors or differences. In addition, the influence of the following boundary conditions is analyzed: the inlet velocity and the intensity of the incoming heat flow or minor chemical species injection. Depending on the value of the total viscous dissipation weighting coefficient, two different flow patterns appear and the robustness of the transition between these two regimes is analyzed.

## 2. Numerical method

Two types of diffusion processes in a convective flow are analyzed: heat transfer on the one hand and mass diffusion of a chemical minor species on the other hand. The corresponding equations are presented below.

### 2.1. Governing equations

We consider the incompressible steady-state two-dimensional flow of a Newtonian fluid with constant properties. The corresponding mass and momentum conservation equations are the following:

$$\nabla \cdot \mathbf{V} = 0 \quad (1)$$

$$\rho \mathbf{V} \cdot \nabla \mathbf{V} = -\nabla P + \mu \nabla^2 \mathbf{V} + \mathbf{F} \quad (2)$$

In this set of equations,  $\mathbf{V}$  is the velocity vector of the fluid,  $\rho$  its density,  $P$  its pressure,  $\mu$  its dynamic viscosity and  $\mathbf{F}$  is a volume force field that will be used in the optimization process described below:  $\mathbf{F}$  can be considered as a virtual force field allowing the velocity field to be varied in order to examine all possible flow configurations and find the one that minimizes the objective functional (and respects the conservation equations and boundary conditions), without a priori on its

pattern. The practical realization of the resulting optimal velocity field can be approached by passive means, such as baffles placed in the fluid path, or by the use of porous materials as described in [36] and [35].

Depending on the diffusion process, the transported scalar is respectively the temperature (for heat transfer) or the mass fraction of the minor species (for mass transfer).

In the case of heat transfer, viscous heating and gravity are neglected and there is no source term in the energy equation nor any radiative exchange. The energy equation writes:

$$\mathbf{V} \cdot \nabla T = \frac{k}{\rho C_p} \nabla^2 T \quad (3)$$

where  $T$  is the fluid temperature,  $k$  its thermal conductivity and  $C_p$  its thermal capacity at constant pressure.

In the case of mass diffusion, a two species high dilution ideal solution is considered and the diffusion equation writes:

$$\mathbf{V} \cdot \nabla w_1 = D \cdot \nabla^2 w_1 \quad (4)$$

where  $w_1$  is the mass fraction of the minor species and  $D$  is the diffusion coefficient. Eqs. 3 and 4 have similar mathematical form and differ in the diffusivity coefficient physical meaning and magnitude.

In the case of heat transfer, the local entropy generation rate (by unit of volume, which is expressed by the triple prime superscript notation) can be calculated using the following expression, where  $\Phi$  is the viscous dissipation function [33] and  $u$  and  $v$  are the longitudinal and normal (to the heated wall) components of the velocity respectively:

$$\dot{S}_{gen}''' = \frac{k}{T^2} (\nabla T)^2 + \frac{\Phi}{T} \quad (5)$$

$$\Phi = \mu \left\{ 2 \left[ \left( \frac{\partial u}{\partial x} \right)^2 + \left( \frac{\partial v}{\partial y} \right)^2 \right] + \left( \frac{\partial u}{\partial y} + \frac{\partial v}{\partial x} \right)^2 \right\} \quad (6)$$

Equation 5 is obtained by considering a finite-size control volume  $\Delta x \Delta y \Delta z$  located at any position in the flow field and small enough so that the thermodynamic state inside the control volume may be regarded as homogeneous. The first and second laws of thermodynamics as well as the fundamental relation  $du = T ds - Pd(1/\rho)$  ( $u$  and  $s$  being the specific internal energy and entropy respectively) are applied to this control volume considered as an open system to deduce the local equation  $\dot{S}_{gen}''' = -(1/T^2) \mathbf{q} \cdot \nabla T + \Phi/T$ , where  $\mathbf{q}$  is the heat flux vector. The heat transfer being carried out

by thermal conduction, the Fourier law  $\mathbf{q} = -k\nabla T$  is applied and Eq. 5 is deduced, revealing two causes of local irreversibility: viscous (linked to the dynamic viscosity  $\mu$ ) and conductive (linked to the thermal conductivity  $k$ ) as underlined in [33].

In the case of mass diffusion, the expression of the local entropy generation rate is more complex [41] and takes into account the existence of two species in the fluid:

$$\dot{S}_{gen}''' = \frac{\rho^2 \bar{R} D}{\bar{M}_1 \bar{M}_2 w_1 (1 - w_1) \bar{c}} (\nabla w_1)^2 + \frac{\Phi}{T} \quad (7)$$

In Eq. 7,  $\bar{R}$  is the (molar) ideal gas constant,  $\bar{M}_1$  and  $\bar{M}_2$  are the molar masses of the minor species and of the solvent respectively and  $\bar{c}$  is the total molar concentration in [ $mol.m^{-3}$ ], which is assumed to be constant for the high dilution ideal solution.

## 2.2. Variational problem

Since the aim is to minimize the entropy generation rate due to the diffusion phenomenon while taking into account the total viscous dissipation, it is reasonable to consider a linear combination of these two terms. The objective functionals to be minimized are provided in Eqs. 8 and 9, corresponding to the case of heat transfer and mass diffusion respectively ( $\Omega$  being the control volume domain):

$$J = \iiint_{\Omega} \left( \frac{k}{T^2} (\nabla T)^2 + W_{\Phi} \Phi \right) d\Omega \quad (8)$$

$$J = \iiint_{\Omega} \left( \frac{\rho^2 \bar{R} D}{\bar{M}_1 \bar{M}_2 w_1 (1 - w_1) \bar{c}} (\nabla w_1)^2 + W_{\Phi} \Phi \right) d\Omega \quad (9)$$

Viscous heating has been neglected in the heat equation (Eq. 3) as the simulations are done in the case of very low values of the Brinkman number. This assumption must be changed for high Reynolds number flows or fluids with high viscosity (like oils or polymers, which can also be non-Newtonian). Moreover, although the rate of entropy generation in Eqs. 5 or 7 is the sum of two terms, we consider situations where the entropy generation rate due to viscous friction is negligible when compared to the heat (or mass) transfer part and the objective functional in Eqs. 8 or 9 takes consistently into account the heat or mass transfer contributor only in the entropy generation term:  $\dot{S}_{gen}''' = (k/T^2)(\nabla T)^2$  or  $\dot{S}_{gen}''' = (\rho^2 \bar{R} D)/(\bar{M}_1 \bar{M}_2 w_1 (1 - w_1) \bar{c})(\nabla w_1)^2$ . The second term of the objective functional is  $W_{\Phi} \Phi$ , the product of the weighting factor  $W_{\Phi}$  by the viscous dissipation  $\Phi$ ,

which represents the pressure drop objective in the optimization problem.  $W_{\Phi}$  can be seen as a weighting factor in a multi-objective optimization problem. Minimizing the entropy generation rate and the pressure drop, while these two objectives are contradictory, does not lead to a single solution. The use of a weighting factor allows to find a whole range of optimized trade-offs: with high values of  $W_{\Phi}$ , the emphasis is on the reduction of pressure drop (and more precisely of the total viscous dissipation  $\Phi_{tot}$ , which corresponds to the mechanical power required to maintain the flow). Conversely, small values of  $W_{\Phi}$  correspond to a focus on minimizing the entropy generation rate in the channel. Each value of  $W_{\Phi}$  leads to an optimal velocity field that minimizes differently the two contradictory objectives pursued since they are assigned different weighting factors.

In order to take into account the constraints expressed by Eqs. 1 and 3 or 4, Lagrange multipliers  $\lambda_1$  and  $\lambda_2$  (depending on the position) are introduced. Finally, the Lagrangian criteria to minimize are Eq. 10 for heat transfer and Eq. 11 for mass diffusion.

$$J^* = \iiint_{\Omega} \left\{ \frac{k}{T^2} (\nabla T)^2 + W_{\Phi} \Phi + \lambda_2 \left[ \frac{k}{\rho C_p} \nabla^2 T - \mathbf{V} \cdot \nabla T \right] + \lambda_1 \nabla \cdot \mathbf{V} \right\} d\Omega \quad (10)$$

$$J^* = \iiint_{\Omega} \left\{ \frac{\rho^2 \bar{R} D}{\bar{M}_1 \bar{M}_2 w_1 (1 - w_1) \bar{c}} (\nabla w_1)^2 + W_{\Phi} \Phi + \lambda_2 \left[ D \nabla^2 w_1 - \mathbf{V} \cdot \nabla w_1 \right] + \lambda_1 \nabla \cdot \mathbf{V} \right\} d\Omega \quad (11)$$

The function to be minimized (the entropy generation rate and the viscous dissipation combined linearly in order to cope with a multi-objective optimization problem) is a functional (a function of functions, which is also non-linear) and the solution sought is a set of functions of the position (the velocity vector field and the scalar field) and not a simple number or even a single vector or tensor. These solution fields must also comply with the conservation equations (also non-linear) and the boundary conditions. One way to find the minimum of the functional could be to use iterative search algorithms (starting from an initial possible field and trying to get closer to the minimum by calculating gradients and penalty functions, for example) or methods based on meta-heuristics (such as genetic approaches) [42]. This implies to carry out a potentially high number of resolutions of the fluid flow equations and of evaluations of the objective functional. On the other hand, the

calculus of variations allows to transform the optimization problem into a system of differential equations [43] [44] (the Euler-Lagrange equations) and the optimization is therefore carried out mathematically and not numerically. One single numerical resolution of the resulting differential equation system is then carried out to find the velocity and scalar fields. In this method, the standard procedure for taking into account the equality constraints that must be respected by the solutions (here: the conservation equations) is done using Lagrange multipliers. The continuity equation and the energy conservation (or mass diffusion) equation are thus taken into account by two Lagrange multipliers. Given the presence of the volume force field  $\mathbf{F}$  in the momentum equation, Eq. 2 is taken into account after obtaining the Euler-Lagrange equations. This procedure allows to find the expression of the volume force field  $\mathbf{F}$  that minimizes the objective functional  $J^*$ : it is described in a synthetic way in the following paragraphs and an appendix at the end of the paper provides the details of the calculations.

Making the first variation of  $J^*$  with respect to  $u$  and  $v$  vanish and taking into account the momentum conservation equation (Eq. 2) gives the formula for the volume force field  $\mathbf{F}$  in Eq. 12 and Eq. 13 for heat transfer and mass diffusion respectively.

$$\mathbf{F} = \frac{\lambda_2}{2W_\Phi} \nabla T + \rho \mathbf{V} \cdot \nabla \mathbf{V} \quad (12)$$

$$\mathbf{F} = \frac{\lambda_2}{2W_\Phi} \nabla w_1 + \rho \mathbf{V} \cdot \nabla \mathbf{V} \quad (13)$$

In addition, equaling to zero the first variation of  $J^*$  with respect to  $T$  leads to the transport equation of the  $\lambda_2$  Lagrange multiplier in Eq. 14 and Eq. 15 for the heat transfer and mass diffusion case respectively.

$$\nabla \cdot \left( \rho \mathbf{V} \lambda_2 - \frac{-k}{C_p} \nabla \lambda_2 \right) = \frac{2k\rho}{T} \nabla \cdot \left( \frac{\nabla T}{T} \right) \quad (14)$$

$$\begin{aligned} & \nabla \cdot [\rho \mathbf{V} \lambda_2 - (-\rho D) \nabla \lambda_2] = \\ & \frac{\rho^3 \bar{R} D}{\bar{M}_1 \bar{M}_2 w_1 (1 - w_1) \bar{c}} \left[ \nabla \cdot \left( \frac{\nabla w_1}{w_1 (1 - w_1)} \right) + \frac{\nabla \cdot (\nabla w_1)}{w_1 (1 - w_1)} \right] \end{aligned} \quad (15)$$

The boundary conditions to be used for Eqs. 14 or 15 depend on those defined for the transported scalar (the temperature or the mass fraction of the minor species): if the scalar function is set at a boundary (Dirichlet condition), Eq. 16 applies. On the other hand, if the flux density of the scalar function is set at the boundary (Von

Neumann condition), Eq. 17 or Eq. 18 are used for heat transfer and mass diffusion respectively.

$$\lambda_2 = 0 \quad (16)$$

$$\frac{\partial \lambda_2}{\partial n} = \frac{2\rho C_p}{T^2} \frac{\partial T}{\partial n} \quad (17)$$

$$\frac{\partial \lambda_2}{\partial n} = \frac{\rho^2 \bar{R}}{\bar{M}_1 \bar{M}_2 \bar{c}} \frac{2}{w_1 (1 - w_1)} \frac{\partial w_1}{\partial n} \quad (18)$$

In these equations,  $\partial/\partial n$  is the normal derivative to the boundary.

Finally, in the case of heat transfer, for each selected value of the  $W_\Phi$  weighting coefficient, Eqs. 1, 2, 3, 12 and 14 are solved with the boundary conditions 16 or 17 complemented by the dynamical and thermal boundary conditions. In the case of mass diffusion, the solved equations are Eqs. 1, 2, 4, 13 and 15 and the boundary conditions are Eqs. 16 or 18 complemented by the dynamical and mass fraction boundary conditions.

For a fixed force field (e.g. if  $\mathbf{F} = 0$  or any other value that may be non-uniform) and for given boundary conditions, Eqs. 1 and 2 determine a single velocity field dependent on the selected field  $\mathbf{F}$ , and Eq. 3 or 4 lead to the corresponding unique scalar field. These velocity and scalar fields determine the value of the total entropy generation rate and the total viscous dissipation. In this paper, the volume force field  $\mathbf{F}$  is considered as an unknown of the optimization problem and the calculus of variations is used to find directly the expression (in Eqs. 12 or 13) of  $\mathbf{F}$  that leads to the velocity and temperature fields minimizing the objective functional.

To summarize, in this paper, optimal theoretical velocity fields are obtained by minimizing the entropy generation rate for different values of the mechanical power required to maintain fluid flow (by varying the weighting factor  $W_\Phi$ ). These suggested velocity fields provide a target to be approached using passive physical means like porous media or modifications of the geometry inside the channel. They also provide a better understanding of how flow structures are related to the minima of entropy generated and the values of the total viscous dissipation. The volume force field  $\mathbf{F}$  is a virtual force allowing to vary the velocity field pattern in order to find the one that minimizes the objective functional.

### 2.3. Numerical model

The fluid is water (a pure substance when the heat transfer case is considered and a highly dilute solution where water is the solvent when the mass diffusion case

is studied). The domain dimensions are  $30\text{ mm} \times 5\text{ mm}$  and a  $1200 \times 200$  uniform mesh is used (Fig. 1). Mesh independence checks have been performed with  $2400 \times 400$  and  $3600 \times 600$  meshes and are described in section 3.3. The top and bottom plates are impermeable and the no-slip boundary condition is applied. The inlet velocity  $V_{in}$  is uniform and constant and the gage pressure is set to zero at the outlet. In the case of heat transfer, the inlet temperature is set to  $T_{in} = 300\text{ K}$  and the walls are adiabatic except for the middle third of the lower plate where a uniform and constant surface heat flux density  $q''$  is set to  $15000\text{ W.m}^{-2}$  unless otherwise indicated. In the case of mass diffusion, the inlet mass fraction of the minor species is set to a fixed value  $w_{1,in} = 0.01$  unless otherwise stated and the middle third of the lower wall is subjected to a fixed production rate per unit area of the minor species  $\dot{m}_1$  set to  $0.01\text{ kg.m}^{-2}.s^{-1}$  unless otherwise indicated.

The CFD code is ANSYS Fluent 15.0 with the SIMPLE velocity-pressure coupling algorithm. UDF scripts have been developed to solve the additional transport equation (14 or 15) and to define the source terms (in particular the  $\mathbf{F}$  volume force field that is applied in the central region of the domain).

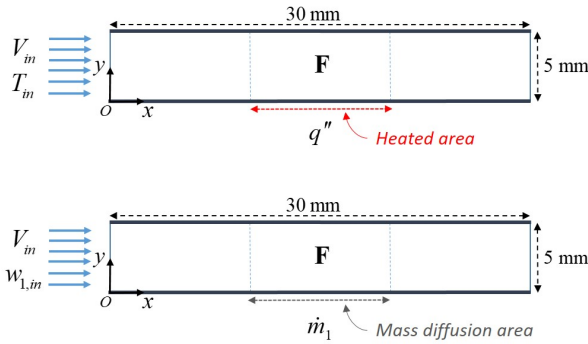


Figure 1: Domain characteristics.

Second-order discretization schemes are used for pressure and energy. Momentum and  $\lambda_2$  equations are solved with a QUICK scheme.

In the present paper, 2D flows have been considered. Two-dimensional simulations can be useful in the case of high aspect ratio cross-sections with a large transversal dimension with respect to the height of the channel (which are considered in the context of solar receivers in concentrating solar power plants, for example). The method discussed in this paper can be applied to three-dimensional flows while requiring significantly more computational resources. The analysis carried out in two dimensions enables to establish qualitative be-

haviors that are likely to persist in three dimensions (for laminar flows) and will facilitate identifying the work to be carried out for three-dimensional flows.

In total, about a hundred simulations were performed to simulate heat transfer or mass diffusion situations, with different values of the  $W_{\phi}$  weighting coefficient that spans across four orders of magnitudes. Moreover, several parameters have been varied in order to analyze their influence: the inlet velocity, the heat flux density (in the heat transfer case), the mass flux density and the inlet mass fraction of the minor species (in the mass diffusion case).

### 3. Results and discussion

#### 3.1. Heat transfer optimization

In this section, we consider the heat transfer case where the channel is heated from the middle third of its bottom plate with a constant and uniform heat flux density  $q''$ . The mass diffusion case will be examined later in section 3.2.

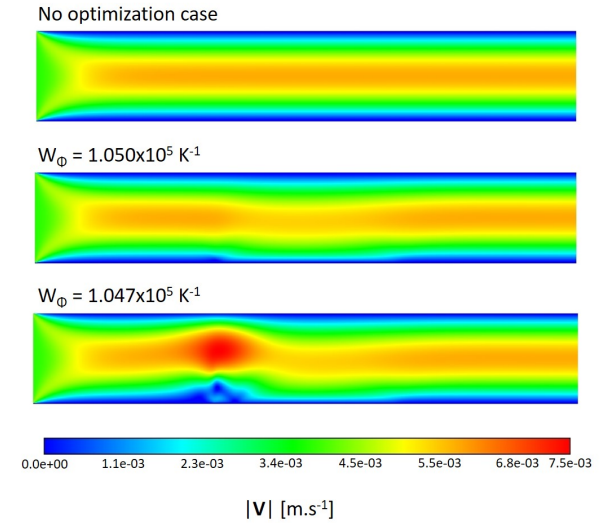


Figure 2: Velocity magnitude fields with no optimization, slightly and highly perturbed profiles ( $Re = 20$ ).

Depending on the importance of the weighting factor  $W_{\phi}$ , the velocity (Fig. 2) and temperature (Fig. 3) fields exhibit different shapes corresponding to flow regimes more or less perturbed when compared to a reference simulation for which no optimization is activated (i.e. when the applied volume force field  $\mathbf{F}$  is zero) [40]. For very large values of  $W_{\phi}$  (for example, when  $W_{\phi} = 10^7\text{ K}^{-1}$ ) these fields are very close to those obtained without optimization. For smaller  $W_{\phi}$  values,

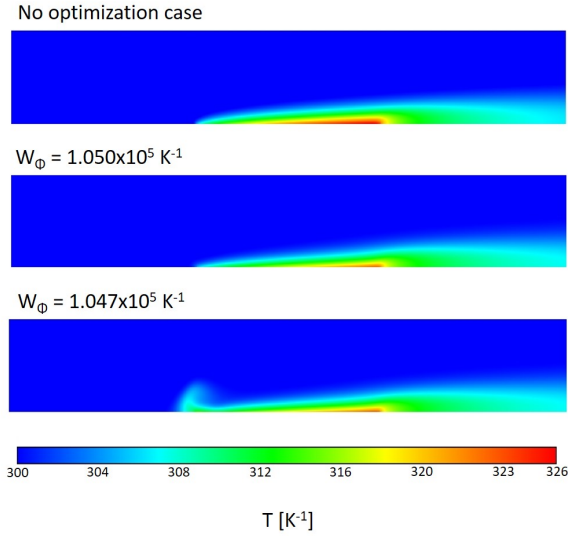


Figure 3: temperature fields with no optimization, slightly and highly perturbed profiles ( $Re = 20$ )

like  $W_{\phi} = 1.05 \times 10^5 K^{-1}$ , the fields are modified without being disrupted: in particular, the flow is slightly pressed against the heated area. For even smaller  $W_{\phi}$  values, for example  $W_{\phi} = 1.047 \times 10^5 K^{-1}$ , the temperature and velocity profiles are clearly perturbed compared to the situation without optimization: the fluid is still pushed towards the heated zone but a clockwise vortex also appears (Fig. 4) that tends to capture the heated fluid at the beginning of the heat exchange zone near the lower plate to move it up in the channel and then accelerate it, before pushing it towards the lower plate. This velocity field results in a thermal plume shape at the beginning of the heated zone. The presence of a vortex in the velocity field resulting from variational optimization is also observed in other physical situations, such as the improvement of chemical reaction [38] or diffusion [36] processes and the optimization of heat transfer in a turbulent gas flow [35]. Vortex generation is also a subject of numerical simulation [9] and experimental [8] work aimed, for example, at associating and optimizing actuators and riblets to produce vortices.

The transition from a low to a highly perturbed regime occurs around a critical value of  $W_{\phi}$  that depends in particular on the Reynolds number. When  $Re = 10$ , the transition takes place around  $W_{\phi} = 2.53 \times 10^5 K^{-1}$  while for  $Re = 20$  it occurs around  $W_{\phi} = 1.05 \times 10^5 K^{-1}$ . As can be seen in Figs. 2 and 3, a small change in the  $W_{\phi}$  value can lead to a significant change in flow: when  $Re = 20$ , reducing  $W_{\phi}$  by

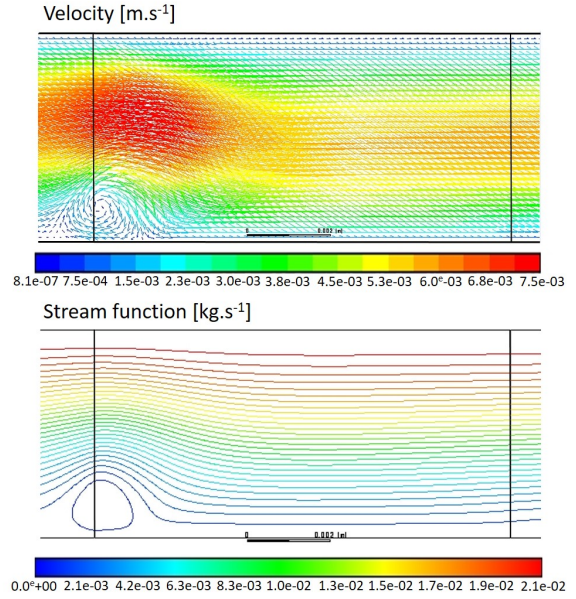


Figure 4: Zoom of velocity vector and stream function fields when  $W_{\phi} = 1.047 \times 10^5 K^{-1}$ . The vertical lines materialize the abscissa  $x = 10 mm$  and  $x = 20 mm$  of the heated region.  $Re = 20$ .

about 0.3 % is enough to induce the transition. Due to this relatively abrupt change, the evolutions of the key variables in the channel (such as the total entropy generated) as a function of  $W_{\phi}$  show a disruption.

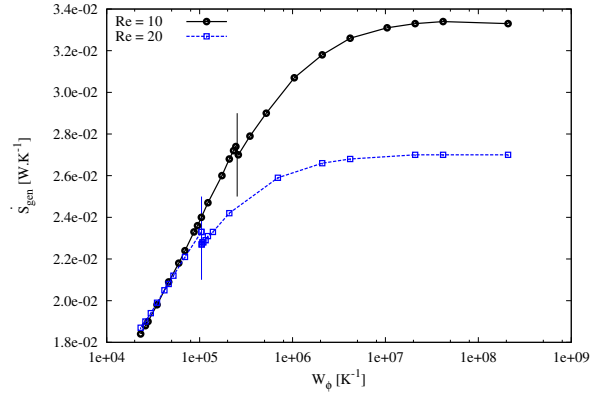


Figure 5: Entropy generation rate as a function of  $W_{\phi}$ .

When the optimization is applied (i.e. the force field  $\mathbf{F}$  is computed and used in the momentum equation), the total entropy generated in the channel is smaller than the case with no optimization (see Fig. 5 where the two vertical bars materialize the critical  $W_{\phi}$  values triggering the transition between the slightly to the highly perturbed velocity and temperature profiles). The re-

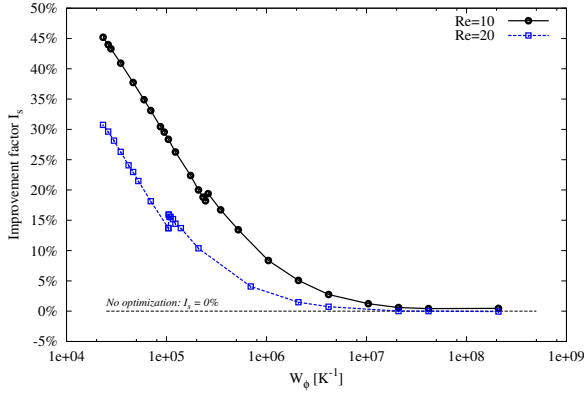


Figure 6: Improvement factor (Eq. 19) as a function of  $W_\Phi$ .

duction in entropy generated is all the more important as  $W_\Phi$  is small and the gain obtained compared to the case without optimization can be estimated using an improvement factor  $I_S$  defined in Eq. 19 and presented in Fig. 6. When  $Re = 20$  and  $W_\Phi = 2.3 \times 10^4 K^{-1}$ ,  $I_S \approx 30\%$  and the total entropy generation rate in the channel is about 70% of non-optimized case. For high values of  $W_\Phi$ , decreasing this factor by one order of magnitude leads to a small (or even zero) marginal gain in entropy rate reduction. On the other hand, when  $W_\Phi$  approaches its critical value and below this point, the slope of the marginal gain is higher (around  $8 mW.K^{-1}$  by order of magnitude of  $W_\Phi$ ).

$$I_S = 1 - \frac{\dot{S}_{gen, optimized}}{\dot{S}_{gen, no optimization}} \quad (19)$$

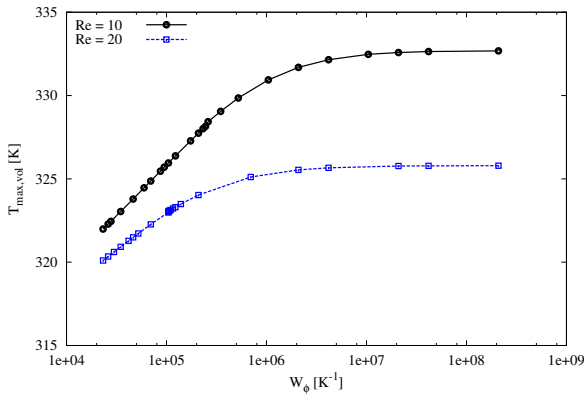


Figure 7: Maximum temperature in the channel as a function of  $W_\Phi$ .

As can be seen in Fig. 7, the maximum temperature inside the channel decreases significantly as  $W_\Phi$  declines and for medium values of  $W_\Phi$  the curve slope

increases when the Reynolds number decreases. The velocity fields resulting from the optimization increase the homogeneity of the temperature field: the standard deviation of the temperature is reduced from  $3.74 K$  to  $3.32 K$  when  $W_\Phi$  changes from  $2.09 \times 10^8 K^{-1}$  to  $1.047 \times 10^5 K^{-1}$  at  $Re = 20$ .

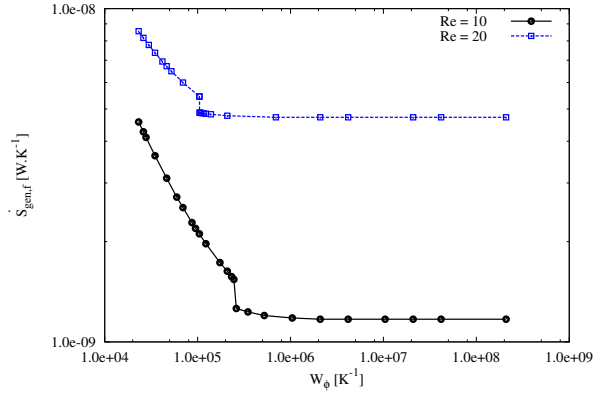


Figure 8: Entropy generation rate due to viscous friction as a function of  $W_\Phi$ .

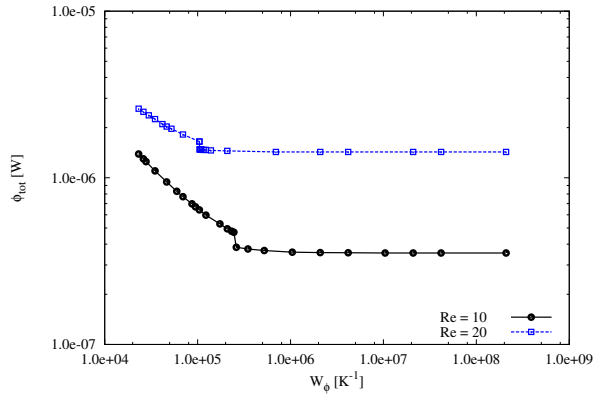


Figure 9: Total viscous dissipation as a function of  $W_\Phi$ .

The entropy generation rate by viscous friction increases as  $W_\Phi$  decreases (Fig. 8) and so does the total viscous dissipation  $\Phi_{tot}$  (Fig. 9) and the maximum velocity within the flow (Fig. 10). The order of magnitude of the viscous friction entropy generation rate  $\dot{S}_{gen,f}$  (between  $1 nW.K^{-1}$  and  $10 nW.K^{-1}$ , depending on the Reynolds number) is much lower than that of the heat conduction entropy generation rate  $\dot{S}_{gen,c}$  ( $10 mW.K^{-1}$ ), which is by far the main contributor to the total entropy generation rate  $\dot{S}_{gen} = \dot{S}_{gen,c} + \dot{S}_{gen,f}$ . The smaller  $W_\Phi$ , the higher the velocities in the channel, leading to increased velocity gradients, viscous dissipation and gen-

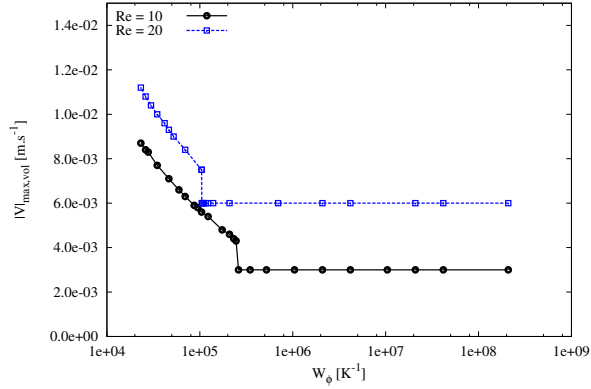


Figure 10: Maximum velocity magnitude in the channel as a function of  $W_\Phi$ .

eration of entropy of viscous origin. At the same time, the better thermal mixing obtained with the optimized velocity fields results in a reduction in entropy generation by thermal conduction through finite temperature differences. The two components of the entropy generation rate evolve in opposite directions. However, since heat conduction entropy generation is the overwhelming majority, decreasing  $W_\Phi$  ultimately results in a decrease in the total entropy generation rate.

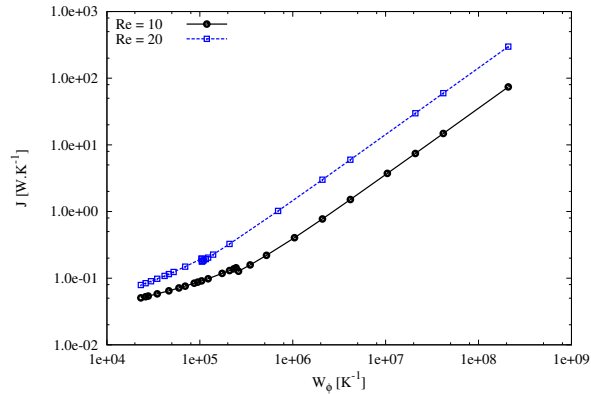


Figure 11: Objective functional  $J$  as a function of  $W_\Phi$ .

The objective functional defined in Eq. 8 decreases as  $W_\Phi$  gets smaller (Fig. 11). It is a linear combination of two terms,  $\dot{S}_{gen,c} \approx \dot{S}_{gen}$  and  $\Phi_{tot}$  that evolve in opposite ways when  $W_\Phi$  varies (Fig. 12). Taking the case  $Re = 20$  as an example, when  $W_\Phi$  falls by approximately four orders of magnitude from  $2.1 \times 10^8 K^{-1}$  to  $2.3 \times 10^4 K^{-1}$ , the entropy generation rate by heat conduction decreases from  $27 mW.K^{-1}$  to  $19 mW.K^{-1}$  and the total viscous dissipation raises from  $1.43 \mu W$  to

$2.60 \mu W$ . Since the entropy generation by heat conduction and the total dissipation do not change their order of magnitude, the evolution of  $W_\Phi$  has the decisive effect and leads to a decrease of the objective functional.

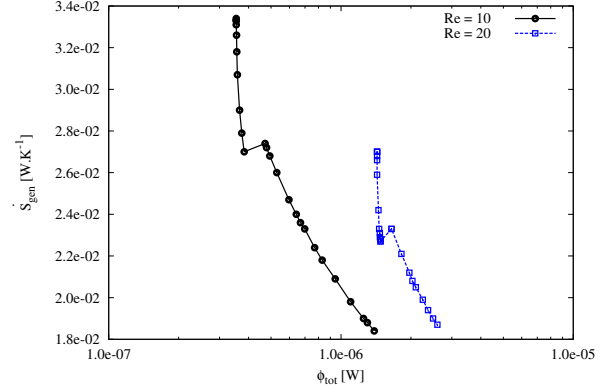


Figure 12: Total entropy generation rate as a function of the total dissipation.

The boundary conditions have an effect on the optimized solutions. the influence of the heat flux density  $q''$  and of the inlet velocity  $V_{in}$  are discussed below.

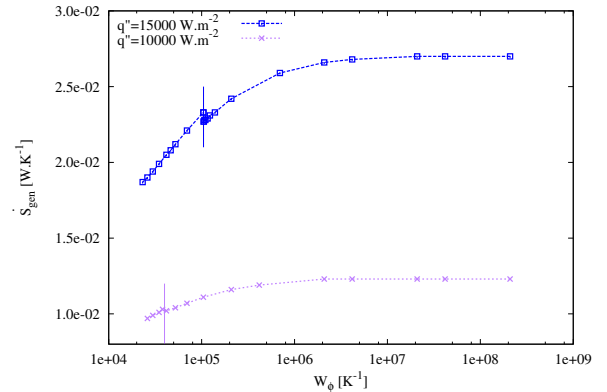


Figure 13: Total entropy generation rates as a function of  $W_\Phi$  for two values of the input heat flux.  $Re = 20$ .

The higher the heat flux density, the higher the entropy generation rate by heat conduction and the higher the total entropy generation rate in the channel (Fig. 13). The critical value of  $W_\Phi$  is lower for a reduced heat flux density: when  $Re = 20$ , changing the heat flux boundary condition from  $15000 W.m^{-2}$  to  $10000 W.m^{-2}$  leads to a fall of the critical  $W_\Phi$  from about  $1 \times 10^5 K^{-1}$  to  $4 \times 10^4 K^{-1}$ . This change in the critical  $W_\Phi$  values directly affects the behavior of the entropy generation rate by viscous friction (Fig. 14) as well as the maximum velocity in the channel (Fig. 15): as long as  $W_\Phi$

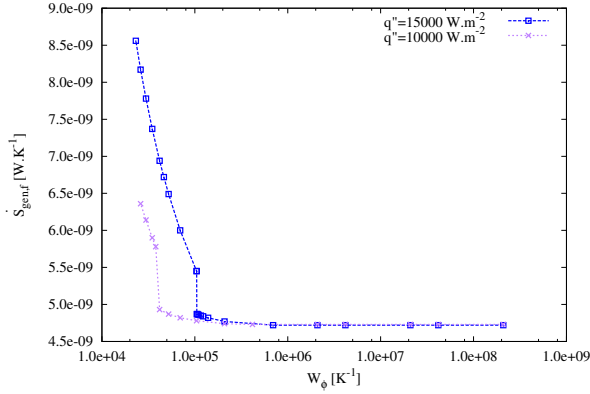


Figure 14: Total entropy generation rates by viscous friction as a function of  $W_\Phi$  for two values of the input heat flux.

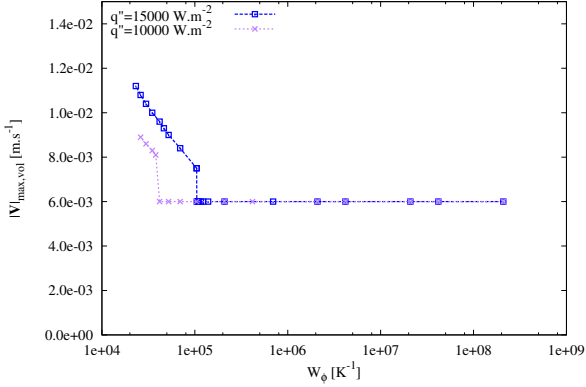


Figure 15: Maximum velocity magnitude in the channel as a function of  $W_\Phi$  for two values of the input heat flux.

is large enough, these two quantities are almost independent of the value of the flow density applied to the heated wall. On the other hand, as soon as  $W_\Phi$  falls below the highest critical value (here, the one corresponding to  $15000 \text{ Wm}^{-2}$ ), the curves are dissociated and the rate of generation of viscous entropy is higher in the case where  $q'' = 15000 \text{ Wm}^{-2}$  compared to that where  $q'' = 10000 \text{ Wm}^{-2}$ .

For a fixed  $W_\Phi$  value, a reduction in the heat flux density applied to the wall results in a reduction in the rate of entropy generation by heat conduction and therefore in the rate of total entropy generation (Fig. 16), the conductive component still remaining largely dominant in the entropy generation mix when compared to the viscous component. Similarly, the maximum temperature reached inside the channel decreases with the imposed heat flow density (Fig. 17). The maximum velocity reached in the channel as well as the rate of vis-

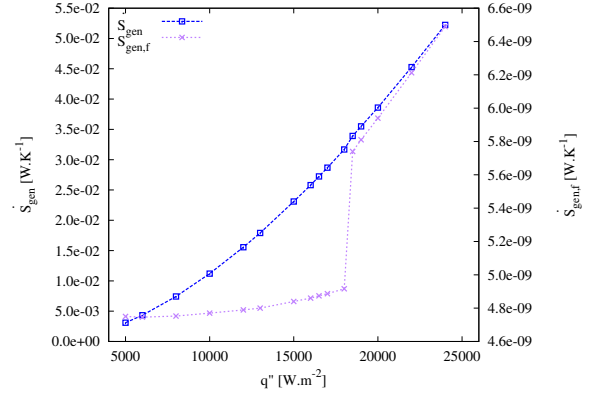


Figure 16: Total and viscous entropy generation rates as functions of the heat flux input from the bottom of the channel ( $Re = 20$  and  $W_\Phi = 1.23 \times 10^5 \text{ K}^{-1}$ ).

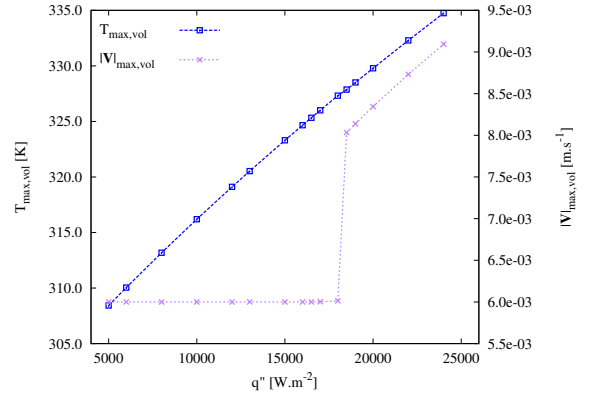


Figure 17: Maximum temperature and maximum velocity magnitude in the channel ( $Re = 20$  and  $W_\Phi = 1.23 \times 10^5 \text{ K}^{-1}$ ).

cus entropy generation also decrease as the imposed heat flux density is reduced (while keeping  $Re$  and  $W_\Phi$  fixed). For high values of  $q''$ , the flow regime is of the highly perturbed type when compared to the case without optimization, whereas for a small applied heat flux density, the flow regime is of the slightly or very slightly perturbed type. The transition between the two regimes, visible in Figs. 16 and 17 takes place for a critical value  $q''_{critical}$ , which is about  $18000 \text{ Wm}^{-2}$  for  $Re = 20$  and  $W_\Phi = 1.23 \times 10^5 \text{ K}^{-1}$ . Indeed, as observed during the examination of Figs. 13 to 15, a reduction in the heat flux density applied to the heated wall leads to a reduction in the critical value of  $W_\Phi$ . As a result,  $W_\Phi$  being set to a given value  $W_{\Phi,0}$  ( $= 1.25 \times 10^5 \text{ K}^{-1}$  for example), reducing  $q''$  from a value corresponding to a highly perturbed ( $24000 \text{ Wm}^{-2}$ ) regime ends up making  $W_\Phi_{critical}(q'')$  coincide with  $W_{\Phi,0}$ , which induces the

transition to a low perturbed flow regime where viscous entropy generation rates and maximum velocities are lower and stabler.

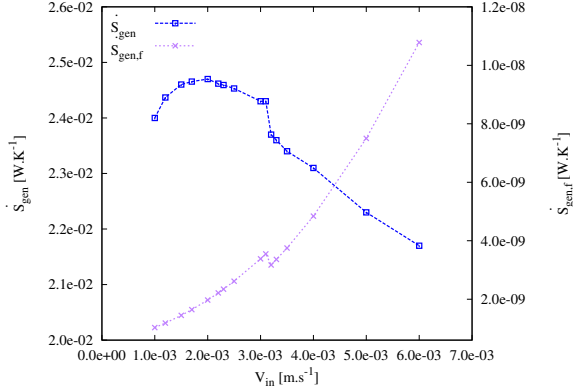


Figure 18: Total and viscous entropy generation rates as functions of  $V_{in}$  ( $W_{\Phi} = 1.23 \times 10^5 K^{-1}$ ).

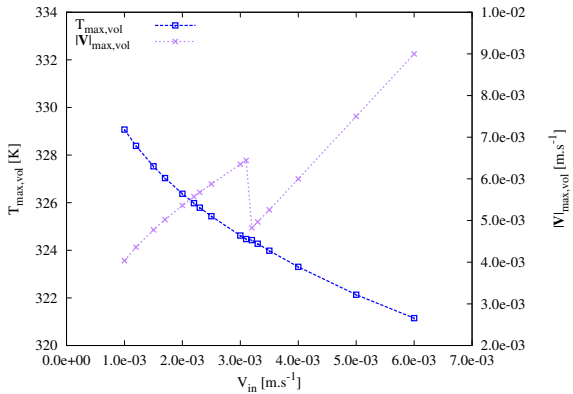


Figure 19: Maximum velocity magnitude and maximum scalar value in the channel as functions of  $V_{in}$  ( $W_{\Phi} = 1.23 \times 10^5 K^{-1}$ ).

If now  $W_{\Phi}$  is fixed (at  $1.23 \times 10^5 K^{-1}$ ) and  $q''$  is also fixed (at  $15000 W.m^{-2}$ ) while varying the inlet velocity  $V_{in}$  between  $6 mm.s^{-1}$  ( $Re \approx 30$ ) and  $1 mm.s^{-1}$  ( $Re \approx 5$ ), one can observe that the entropy generation rate of viscous origin as well as the maximum velocity in the flow decrease with  $V_{in}$  (Figs. 18 and 19). However, the maximum velocity curve exhibits a significant disruption: a transition appears for a critical value  $V_{in,critical}$  approximately equal to  $3.2 mm.s^{-1}$  ( $Re = 15.8$ ) between highly perturbed flow regimes (when the inlet velocity is lower than  $V_{in,critical}$ ) and slightly perturbed ones. Indeed, as already observed in Fig. 5, a reduction in the Reynolds number leads to an increase of the critical  $W_{\Phi}$ . If one sets  $W_{\Phi}$  to a fixed value  $W_{\Phi,0}$  and reduces the inlet

velocity, there is a point where the increasing critical weighting parameter  $W_{\Phi,critical}(V_{in})$  reaches the value  $W_{\Phi,0}$  and triggers the transition from slightly to highly perturbed profiles.

At fixed  $W_{\Phi}$  and  $q''$ , lowering the inlet velocity leads to an increase of the maximum temperature in the channel (Fig. 19). The total entropy generation rate also grows as  $V_{in}$  decreases with the exception of a behavior change for very small inlet velocities (when  $V_{in} \leq 2 mm.s^{-1}$ ) as exhibited in Fig. 18.

### 3.2. Mass transfer optimization

In this section, we consider the mass transfer case where at the middle third of the bottom plate a minor species diffuses at a constant and uniform mass production time rate by unit of surface  $\dot{m}_1$ . The objective is to verify if the behaviors described in section 3.1 are similar in a different advection-diffusion phenomenon but with close mathematical model. The comparison between heat and mass transfer simulations is done at the same Reynolds number  $Re = 10$ .

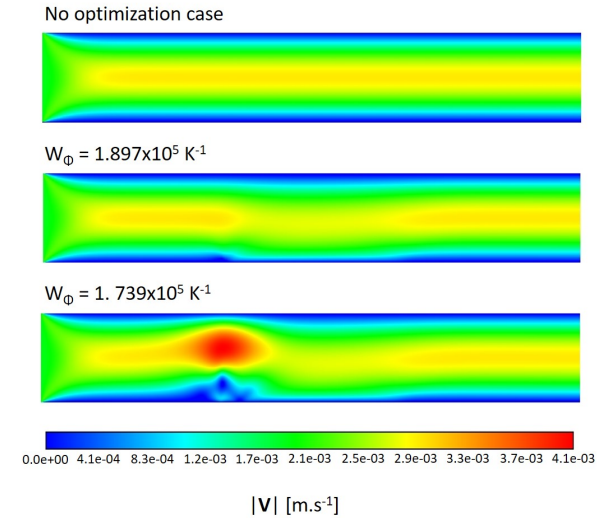


Figure 20: Velocity magnitude with no optimization, slightly and highly perturbed profiles ( $Re = 10$ ).

First, one finds again the presence of slightly and highly perturbed flow regimes (Figs 20 and 21) when compared to the non-optimized case, whose shapes are very similar to that of the velocity and transported scalar profiles of the heat transfer case (Figs. 2 and 3), the key scalar quantity being here the mass fraction of the chemical minor species whereas this was previously the temperature.

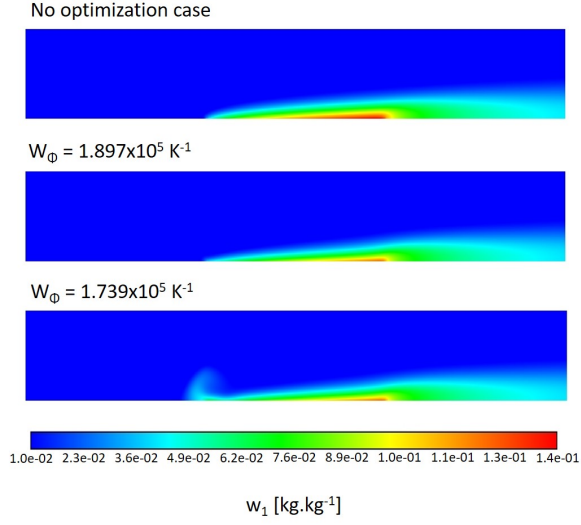


Figure 21: Mass fraction of the minor species with no optimization, slightly and highly perturbed profiles ( $Re = 10$ ).

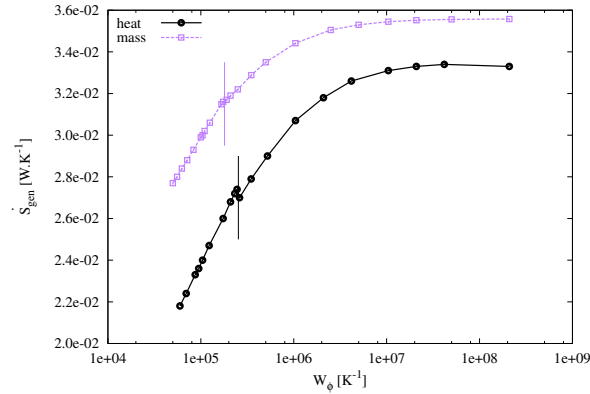


Figure 22: Total entropy generation rate as a function of  $W_\Phi$ .

The evolution of entropy generation and viscous dissipation quantities as a function of the weighting parameter  $W_\Phi$  are presented in Figures 22 to 27 by comparing the case of heat transfer with that of mass diffusion at  $Re = 10$ . A decrease in  $W_\Phi$  leads to a reduction in the total entropy generation rate (Fig. 22) and in the objective functional (Fig. 23), unlike the entropy generation rate by viscous dissipation (Fig. 24) and the total viscous dissipation (Fig. 25) that increase as  $W_\Phi$  decreases. These behaviors are quite similar to those observed previously in the case of heat transfer and it is the same for the relationship between the total entropy generation rate and the total viscous dissipation (Fig. 26). The entropic improvement factor  $Is$  defined in Eq. 19 becomes higher as  $W_\Phi$  gets lower

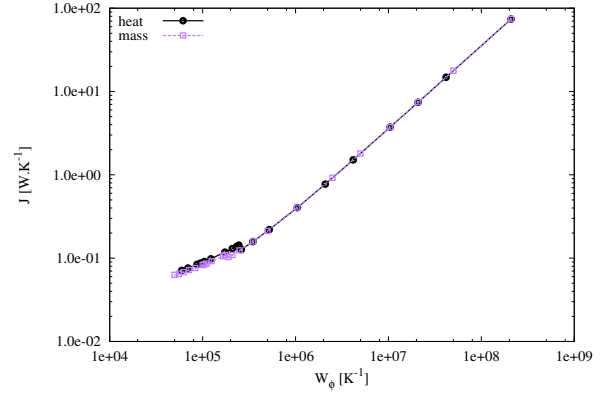


Figure 23: Objective functional  $J$  as a function of  $W_\Phi$ .

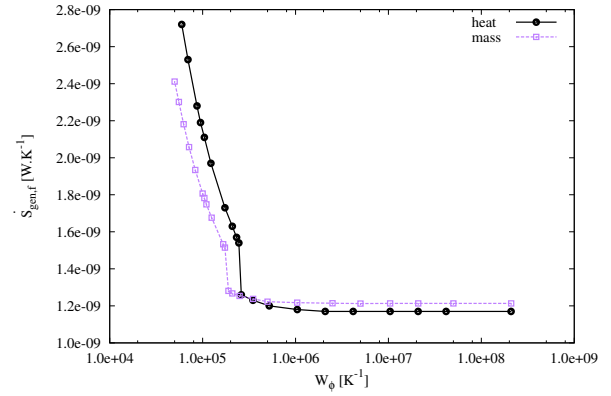


Figure 24: Entropy generation rate due to viscous friction as a function of  $W_\Phi$ .

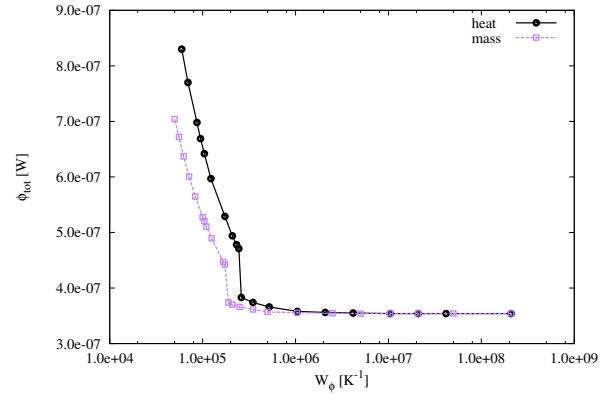


Figure 25: Total viscous dissipation as a function of  $W_\Phi$ .

(Fig. 27). Whether it is a heat transfer case or a mass diffusion case, there is a critical  $W_\Phi$  value that triggers the transition from the slightly perturbed regime (when

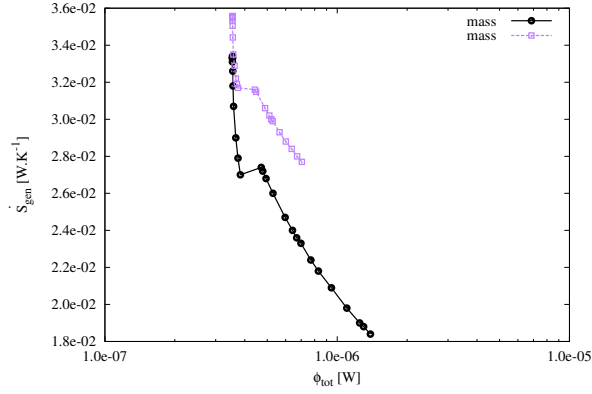


Figure 26: Total entropy generation rate as a function of the total dissipation.

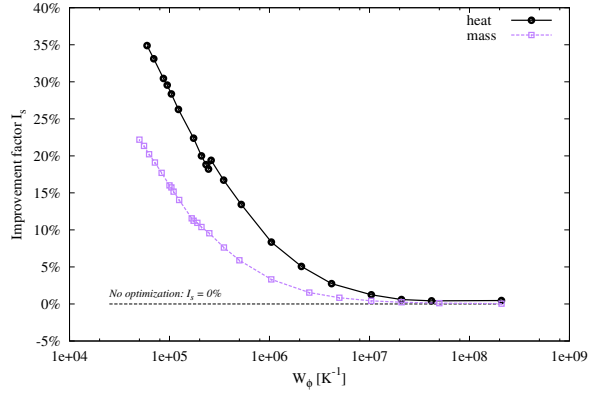


Figure 27: Improvement factor as a function of  $W_\Phi$ .

$W_\Phi$  is large) to the highly perturbed regime (for  $W_\Phi$  smaller than  $W_{\Phi,critical}$ ). The critical value of  $W_\Phi$  is about  $2.5 \times 10^5 K^{-1}$  for the heat transfer case and around  $1.8 \times 10^5 K^{-1}$  for the mass diffusion case. As a conclusion, without being strictly identical, the optimization of heat transfer and mass diffusion exhibit very similar behaviors.

If the value of  $W_\Phi$  is set to  $1.67 \times 10^5 K^{-1}$  at a fixed Reynolds number ( $Re = 10$ ) and the mass production rate at the exchange section of the bottom part of the channel is varied, the total and viscous entropy generation rates have profiles similar to those of heat transfer: all entropy generation rates decrease as the input flux density decreases (Fig. 28). In addition, a critical value of  $\dot{m}_1$  exists, for which the transition takes place between the very disturbed flow regime (for large values of  $\dot{m}_1$ ) and the slightly disturbed regime (below  $\dot{m}_{1,critical} \approx 9 \times 10^{-3} kg.m^{-2}.s^{-1}$ ). As  $\dot{m}_1$  gets lower, the maximum and average mass fraction of the minor

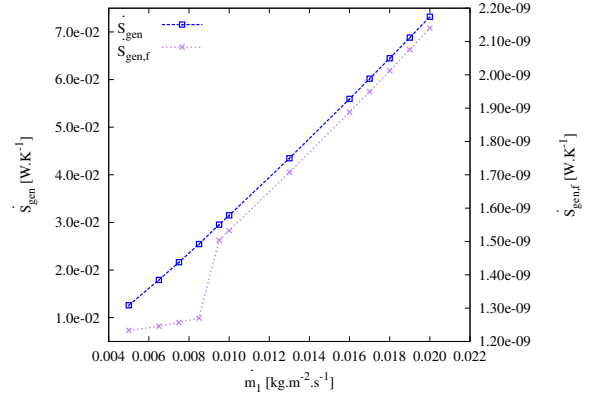


Figure 28: Total and viscous entropy generation rates as functions of the diffusion intensity from the bottom plate ( $W_\Phi = 1.67 \times 10^5 K^{-1}$  and  $Re = 10$ ).

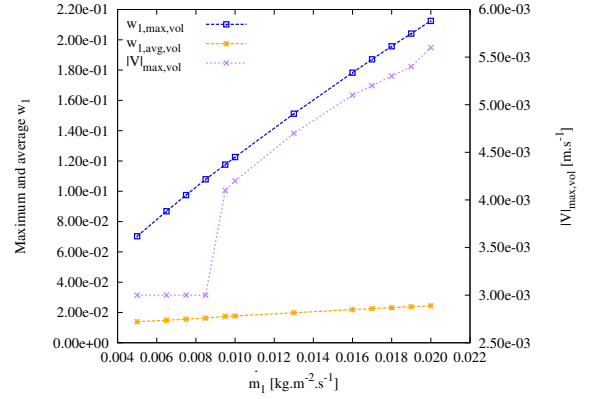


Figure 29: Maximum and average mass fraction of the minor species and maximum velocity as functions of the diffusion intensity from the bottom plate ( $W_\Phi = 1.67 \times 10^5 K^{-1}$  and  $Re = 10$ ).

species decrease as does the maximum velocity in the channel (Fig. 29), which exhibits the disruption at the critical value  $\dot{m}_{1,critical}$ .

If now, for a fixed value of the weighting factor ( $W_\Phi = 1.67 \times 10^5 K^{-1}$ ), the Reynolds number ( $Re = 10$ ) and the bottom plate mass flux density are fixed ( $0.01 kg.m^{-2}.s^{-1}$ ), while varying the minor mass fraction  $w_{1,in}$  at the inlet from  $10^{-5}$  to 0.03, all velocity and mass fraction fields stay in the highly perturbed flow regime and there is no observed critical value of  $w_{1,in}$  in the tested value range. A decrease in the inlet mass fraction of the minor species leads to an increase in all entropy generation rates whether it comes from mass diffusion or from viscous friction (Fig. 30). Correlatively, a lower value of  $w_{1,in}$  corresponds to a reduction in the maximum and the average mass fraction of the minor species in the channel and to an increase of the

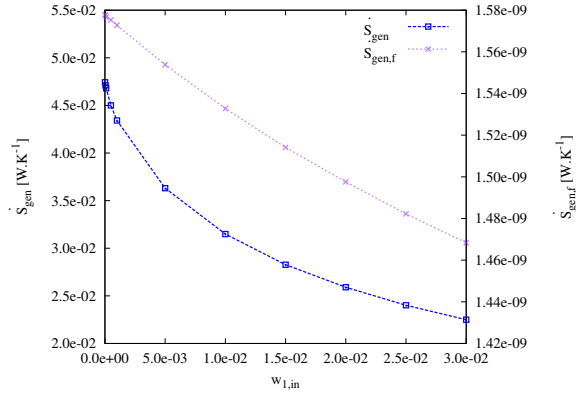


Figure 30: Total and viscous entropy generation rates in the channel as functions the inlet mass fraction of the minor species ( $W_{\Phi} = 1.67 \times 10^5 K^{-1}$  and  $Re = 10$ ).

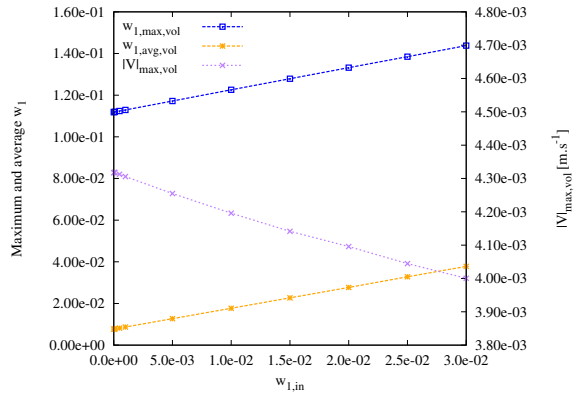


Figure 31: Maximum velocity magnitude in the channel as functions the inlet mass fraction of the minor species ( $W_{\Phi} = 1.67 \times 10^5 K^{-1}$  and  $Re = 10$ ).

maximum velocity (Fig. 31).

### 3.3. Robustness of the transition

600 In sections 3.1 and 3.2, the presence of a regime transition between slightly and highly perturbed velocity and scalar fields has been pointed out, as the existence  
620 of critical values of the  $W_{\Phi}$  weighting parameter in the functional objective that trigger this transition. This has  
605 been observed for different Reynolds numbers, different values of the physical diffusivity coefficients and different  
625 boundary conditions. It is also useful to examine the mesh independence of this regime transition, whether it  
610 depends on initial conditions and what could be its underlying cause.

Keeping the same physical domain size, two finer meshes have been tested for the heat transfer case when  
630  $Re = 20$  and  $q'' = 15 kW.m^{-2}$ : in addition to the base

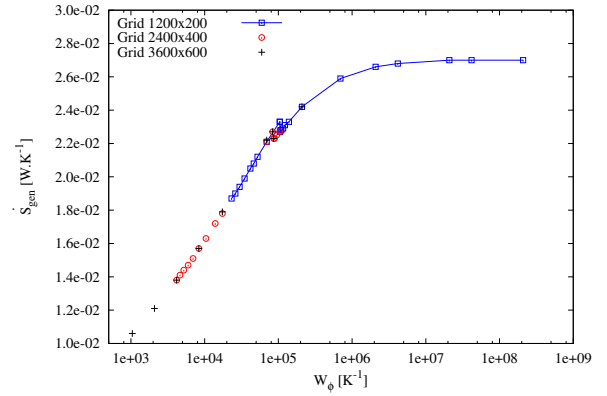


Figure 32: Total entropy generation rate as a function of  $W_{\Phi}$ , complemented by finer mesh simulations.  $Re = 20$ .

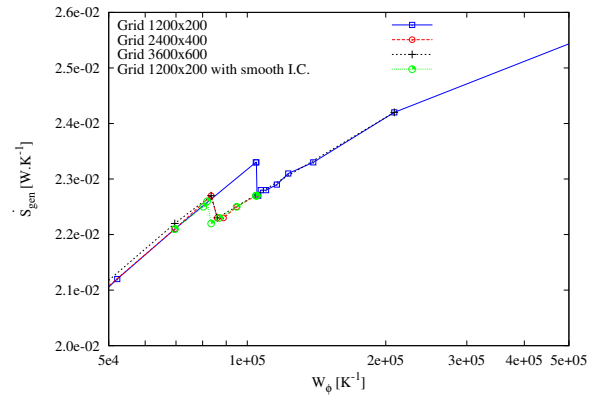


Figure 33: Total entropy generation rate as a function of  $W_{\Phi}$  - zoom on transition zone showing the influence of the grid resolution and the initial conditions (I.C.).  $Re = 20$ .

615 1200×200 mesh, 2400×400 and 3600×600 meshes have been used and the corresponding results for the total entropy generation rate as a function of  $W_{\Phi}$  are presented in Fig. 32. The  $\dot{S}_{gen}$  curve has been extended to smaller values of  $W_{\Phi}$  (down to  $10^3 K^{-1}$ ) and the corresponding extended part of the graph is consistent with the above results: the total entropy generation rate keeps declining as  $W_{\Phi}$  decreases.

A zoom around the critical  $W_{\Phi}$  value is provided in Fig. 33. In the case of finer grids, the critical  $W_{\Phi}$  still exists but at a lower value while keeping the same order of magnitude ( $\approx 8.5 \times 10^4 K^{-1}$  in place of  $\approx 1 \times 10^5 K^{-1}$ ). Furthermore, tests have been performed with the  $1200 \times 200$  mesh by approaching the critical value of  $W_{\Phi}$  step by step in a smooth manner, each simulation starting from the results of the converged previous one with a value of  $W_{\Phi}$  slightly lower (while all the simulations presented above are started from the ho-

635 homogeneous initial conditions where the temperature of the channel is set to  $T_{in}$  and the longitudinal velocity is set to  $V_{in}$ , the normal velocity being zero at the initial time of the simulation). The corresponding results are presented in Fig. 33: the existence of the critical  $W_{\Phi}$  is still confirmed at a value close to the one obtained with the finer grids ( $\approx 8.4 \times 10^4 K^{-1}$ ). So, the existence and the approximate critical  $W_{\Phi}$  value are quite robust. 690

640 For the high values of  $W_{\Phi}$ , the product  $\Phi W_{\Phi}$  is much higher than the diffusion entropy generation rate (by heat conduction or mass diffusion, depending on the type of simulation performed) and the second term of the objective functional is predominant. Conversely, for small values of  $W_{\Phi}$ , the first term of  $J$  in Eq. 8 or 9 is the majority. In the critical value area of  $W_{\Phi}$ , in which the change in flow regime takes place, the two terms composing the objective functional have close orders of magnitude: the difference in orders of magnitude, estimated by  $\text{Log}_{10}(\Phi_{tot} W_{\Phi} / \dot{S}_{gen,d})$ , where  $\dot{S}_{gen,d}$  is the entropy generation rate by diffusion of heat or mass, lies between 0.37 and 0.85 depending on the Reynolds number and the transfer type. The flow regime transition could therefore be related to the fact that the optimization program focuses on viscous dissipation when  $W_{\Phi}$  is large and on entropy generation by heat conduction or mass diffusion when  $W_{\Phi}$  is small. In the second case, the optimized solution can rely on a more complex and intense velocity field to produce a thermal mixture, at the expense of an increase in viscous dissipation which effect on the objective criterion is negligible due to the small size of the  $W_{\Phi}$  factor. The transition from one regime to another would then be linked at least in part to the shift from an optimization focused on viscous dissipation to an optimization focused on entropy generation by diffusion. 705

655 When  $W_{\Phi}$  becomes very large, the first term in Eqs. 12 or 13 cancels and the resulting momentum conservation equation corresponds to that of Stokes flow  $\nabla P = \mu \nabla^2 V$ , for which the advection term is negligible when compared to the viscous term. This corresponds to low Reynolds number flows without optimization. If  $W_{\Phi}$  tends towards zero, the first term in Eqs. 12 or 13 becomes large and leads to a coupling between the pressure, the velocity and the temperature (or the mass fraction of the minor species) in the momentum conservation equation. The smaller  $W_{\Phi}$ , the more intense (in magnitude) and complex the velocity field becomes due to the presence of vortexes in particular. Exploring the behavior of optimized velocity fields for smaller and smaller values of  $W_{\Phi}$  requires working with finer meshes and demands more computing resources. In this paper, we went down as far as  $W_{\Phi} = 10^3 K^{-1}$  (Fig. 32) 730

in order to stay within reasonable limits in terms of computation time, while observing a wide range of values for this weighting parameter. Conversely, large values of the weighting factor (up to  $W_{\Phi} \approx 10^8 K^{-1}$ ) allow to examine the effect of the optimization when the overwhelming emphasis is on reducing (or increasing as little as possible) the pressure drop, even if it means an increase (or a smaller reduction) of the entropy generation rate in the channel.

A discontinuity appears at a precise critical value of the weighting factor. The criterion for identifying  $W_{\Phi,critical}$  is the jump in the maximum velocity within the channel (Figs. 10, 15, 17, 19, 29). Other physical quantities also exhibit a discontinuity for the same value of  $W_{\Phi,critical}$ . This is the case for the entropy generation rates (due to viscous friction in particular) and the total viscous dissipation (Figs. 5, 8, 9, 12, 13, 14, 16, 18, 22, 24, 25, 26, 28). Simultaneously, a change in the pattern of the velocity field occurs at  $W_{\Phi} = W_{\Phi,critical}$  as can be seen in Figs. 2 and 3 or 20 and 21: if  $W_{\Phi}$  is higher than the critical value, the flow streamlines are a little closer to the lower plate above the heated zone but the flow remains close to the one without optimization. We have labeled this configuration as “slightly perturbed” as opposed to the one that appears for  $W_{\Phi}$  below the critical value: in this case, a vortex is present and, as indicated previously, the velocity magnitude increases sharply. We have referred to this second configuration as “highly perturbed”. The present study shows that the critical value  $W_{\Phi,critical}$  depends on the boundary conditions and the Reynolds number in particular. The physical properties of the fluid may surely have an influence, as this critical value seems to correspond to an approximate balance between the two terms of the objective functional (the entropy generation rate in the channel on the one hand and the weighted product  $W_{\Phi}$  times  $\Phi$ , on the other hand). The optimizations carried out in the present work have all been performed at constant physical properties in order to examine in detail the behavior of the method in this first case. This enables to start from initial solutions known in the literature [36] and then to vary the boundary conditions and the optimization parameters. However, the properties of fluids generally depend on temperature. In the case of heat transfer for real water, the dynamic viscosity varies significantly [45] over the temperature range observed in the simulations (from 300K to 335K depending on the Reynolds number or the heat flux density provided - see Figs. 7 and 17). The temperature dependence of viscosity can have an impact on the precise value of the critical weighting factor  $W_{\Phi,critical}$  that determines the transition between different flow regimes. Taking into 735

account thermo-dependent properties involves solving more complex fluid governing equations, as the temperature field would influence the flow dynamics due to the coupling between the energy and momentum equations. In addition, the variational problem is modified and the equations determining the force field  $\mathbf{F}$  are made more complex. A detailed study of the influence of the characteristics of the fluid (including its viscosity and thermal conductivity and their dependence on temperature, in particular) is a research work in itself to be carried out as a continuation of the present work.

#### 4. Conclusion

In the present paper, convective flow transfer is submitted to variational methods in order to find optimized velocity and scalar fields that minimize the entropy generation rate and the total viscous dissipation in a channel. This two-objective optimization is addressed by a linear combination of the two criteria to be minimized using a weighting factor allowing to control the relative importance of the total viscous dissipation in the objective functional. Heat transfer and mass diffusion cases are studied and the influence of the weighting factor on the resulting fields and the key physical quantities is analyzed. The velocity patterns suggested by the optimization program lead to a reduced total entropy generation rate in the channel, the relative improvement being larger as the weighting factor or the Reynolds number are lower. These patterns can be a reference for the design of enhanced exchangers. Improved scalar homogeneity (of the temperature or the minor species mass fraction, depending on the type of transfer) is observed as the scalar maximum value and standard deviation are lower while the weighting factor is reduced. This enhancement is achieved at the expense of an increase in the entropy generation rate by viscous friction, which stays nevertheless at a negligible level. The maximum velocity and the total viscous dissipation also increase when the weighting factor decreases. Two main flow regimes are observed, depending on the level of perturbation of the velocity and scalar fields. In highly perturbed regimes, a more complex flow is observed with a vortex and a displacement of the flow towards the diffusion entry area (the heated segment or the mass diffusion entry zone, depending on the transfer process). The transition from a slightly to a highly perturbed flow is triggered by a critical value of the weighting factor, the highest perturbation level corresponding to the lowest weighting factors. This critical value depends on the Reynolds number, the heat or mass transfer intensity at

the exchange plate and on the inlet velocity. At identical Reynolds number, the optimization of mass diffusion and heat transfer exhibit similar behaviors. The existence of the transition between two perturbation flow regimes and the corresponding critical value of the viscous dissipation weighting factor is confirmed with finer meshes and smoother initial conditions.

#### 5. Acknowledgement

This work was supported by French Investments for the future ("Investissements d'Avenir") programme managed by the National Agency for Research (ANR) under contract ANR-10-LABX-22-01 (labex SOLSTICE) and has received funding from the European Union's Horizon 2020 research and innovation programme under grant agreement No 654663, SOLPART project.

#### 6. Appendix

In this appendix, the transport equation for the  $\lambda_2$  Lagrange multiplier (Eq. 14) and the volume force field  $\mathbf{F}$  (Eq. 12) are found by applying the calculus of variations in the case of heat transfer optimization. The same procedure can be used to obtain the corresponding equations in the case of mass diffusion (Eqs. 15 and 13).

The Lagrangian criterion to minimize writes:

$$\begin{aligned}
 J^* &= \iiint_{\Omega} \left\{ \frac{k}{T^2} (\nabla T)^2 + W_{\Phi} \Phi \right. \\
 &+ \lambda_2 \left[ \frac{k}{\rho C_p} \nabla^2 T - \mathbf{V} \cdot \nabla T \right] + \lambda_1 \nabla \cdot \mathbf{V} \left. \right\} d\Omega \quad (20) \\
 &= \iiint_{\Omega} F_{J^*} d\Omega
 \end{aligned}$$

In this equation, the term to be integrated has been named  $F_{J^*}$  and a compact notation is used in the following calculations: the subscript  $(\cdot)_{,X}$  stands for the derivative with respect to  $X$  and  $(\cdot)_{,XX}$  stands for the second derivative ( $T_{,xx}$  means  $\partial^2 T / \partial x^2$  and  $T_{,x}^2$  means  $(\partial T / \partial x)^2$ ).  $F_{J^*}$  can be rewritten:

$$\begin{aligned}
 F_{J^*} &= \frac{k}{T^2} (T_{,x}^2 + T_{,y}^2) \\
 &+ W_{\Phi} \mu [2(u_{,x}^2 + v_{,y}^2) + (u_{,y} + v_{,x})^2] \\
 &+ \lambda_2 \left[ \frac{k}{\rho C_p} (T_{,xx} + T_{,yy}) - (uT_{,x} + vT_{,y}) \right] \\
 &+ \lambda_1 (u_{,x} + v_{,y})
 \end{aligned} \quad (21)$$

815 For functional in Eq. 20 to have a minimum, its first variation (or differential) must cancel out and making this first variation of  $J^*$  with respect to the temperature vanish implies the following Euler-Lagrange equation [43] [44]:

$$\begin{aligned} \frac{\partial F_{J^*}}{\partial T} - \frac{\partial}{\partial x} \frac{\partial F_{J^*}}{\partial T_{,x}} - \frac{\partial}{\partial y} \frac{\partial F_{J^*}}{\partial T_{,y}} \\ + \frac{\partial^2}{\partial x^2} \frac{\partial F_{J^*}}{\partial T_{,xx}} + \frac{\partial^2}{\partial y^2} \frac{\partial F_{J^*}}{\partial T_{,yy}} = 0 \end{aligned} \quad (22)$$

820 Each term of Eq. 22 writes:

$$\begin{aligned} \frac{\partial F_{J^*}}{\partial T} &= \frac{-2k}{T^3} (T_{,x}^2 + T_{,y}^2) \\ \frac{\partial}{\partial x} \frac{\partial F_{J^*}}{\partial T_{,x}} &= \frac{2k}{T^3} T_{,xx} - \frac{4k}{T^2} T_{,x}^2 - \lambda_2 u_{,x} - u \lambda_{2,x} \\ \frac{\partial}{\partial y} \frac{\partial F_{J^*}}{\partial T_{,y}} &= \frac{2k}{T^3} T_{,yy} - \frac{4k}{T^2} T_{,y}^2 - \lambda_2 v_{,y} - v \lambda_{2,y} \\ \frac{\partial^2}{\partial x^2} \frac{\partial F_{J^*}}{\partial T_{,xx}} &= \frac{k}{\rho C_p} \lambda_{2,xx} \\ \frac{\partial^2}{\partial y^2} \frac{\partial F_{J^*}}{\partial T_{,yy}} &= \frac{k}{\rho C_p} \lambda_{2,yy} \end{aligned} \quad (23)$$

Injecting the above expressions into Eq. 22 and taking into account the continuity equation  $u_{,x} + v_{,y} = 0$  leads to Eq. 24 that can be written in the form of a transport equation for the  $\lambda_2$  scalar (Eq. 25, corresponding to Eq. 14).

$$\begin{aligned} \frac{2k}{T^3} (T_{,x}^2 + T_{,y}^2) - \frac{2k}{T^2} (T_{,xx} + T_{,yy}) + u \lambda_{2,x} + u \lambda_{2,y} \\ + \frac{k}{\rho C_p} (\lambda_{2,xx} + \lambda_{2,yy}) \end{aligned} \quad (24)$$

$$\nabla \cdot \left( \rho \mathbf{V} \lambda_2 - \frac{k}{C_p} \nabla \lambda_2 \right) = \frac{2k\rho}{T} \nabla \cdot \left( \frac{\nabla T}{T} \right) \quad (25)$$

The same method can be used to find the expression of the volume force field  $\mathbf{F}$  by making the first variation of  $J^*$  vanish with respect to the longitudinal and wall-normal components of the velocity ( $u$  and  $v$  respectively) and by using the continuity equation, which leads to:

$$\begin{aligned} \lambda_2 T_{,x} + \lambda_{1,x} + 2W\phi\mu(u_{,xx} + u_{,yy}) = 0 \\ \lambda_2 T_{,y} + \lambda_{1,y} + 2W\phi\mu(v_{,xx} + v_{,yy}) = 0 \end{aligned} \quad (26)$$

These two equations can be combined into a more compact vector equation (Eq. 27) that can be compared

with the momentum equation (Eq. 28), which leads [36] to identify  $\nabla P$  (Eq. 29) and  $\mathbf{F}$  (Eq. 30), the expression searched for the volume force.

$$\frac{-\lambda_2}{2W\phi} \nabla T - \frac{1}{2W\phi} \nabla \lambda_1 = \mu \nabla^2 \mathbf{V} \quad (27)$$

$$\rho \mathbf{V} \cdot \nabla \mathbf{V} + \nabla P - \mathbf{F} = \mu \nabla^2 \mathbf{V} \quad (28)$$

$$\nabla P = -\frac{1}{2W\phi} \nabla \lambda_1 \quad (29)$$

$$\mathbf{F} = \frac{\lambda_2}{2W\phi} \nabla T + \rho \mathbf{V} \cdot \nabla \mathbf{V} \quad (30)$$

## 7. References

- [1] S. Akbarzadeh, M. S. Valipour, Heat transfer enhancement in parabolic trough collectors: A comprehensive review, *Renewable and Sustainable Energy Reviews* 92 (2018) 198–218. doi:10.1016/j.rser.2018.04.093.
- [2] G. Flamant, D. Gauthier, H. Benoit, J.-L. Sans, B. Boissière, R. Ansart, M. Hemati, A new heat transfer fluid for concentrating solar systems: Particle flow in tubes, *Energy Procedia, SolarPACES 2013* 49 (2014) 617–626. doi:10.1016/j.egypro.2014.03.067.
- [3] Y. C. Soo Too, R. Benito, Enhancing heat transfer in air tubular absorbers for concentrated solar thermal applications, *Applied Thermal Engineering* 50 (2013) 1076–1083. doi:10.1016/j.applthermaleng.2012.06.025.
- [4] J. M. Avellaneda, F. Bataille, A. Toutant, DNS of turbulent low Mach channel flow under asymmetric high temperature gradient: Effect of thermal boundary condition on turbulence statistics, *International Journal of Heat and Fluid Flow* 77 (2019) 40–47. doi:10.1016/j.ijheatfluidflow.2019.03.002.
- [5] K. Liu, C. P. Titan, L. A. Carrilho, J. A. Khan, Enhancement of heat transfer performance in nuclear fuel rod using nanofluids and surface roughness technique, *ASME International Mechanical Engineering Congress and Exposition, Volume 8B: Heat Transfer and Thermal Engineering, V08BT10A011*. doi:10.1115/IMECE2015-51476.
- [6] R. Xu, L. Zhang, F. Zhang, P. Jiang, A review on heat transfer and energy conversion in the enhanced geothermal systems with water/CO<sub>2</sub> as working fluid, *International Journal of Energy Research* 39 (2015) 1722–1741. doi:10.1002/er.3352.
- [7] S. K. Saha, M. Tiwari, B. Sundén, Z. Wu, *Advances in Heat Transfer Enhancement*, Springer, 2016, ISBN:978-3-319-29478-0.
- [8] X. Daguene-Frick, J.-M. Foucaut, S. Coudert, A. Toutant, G. Olalde, Experimental analysis of the turbulent flow behavior of a textured surface proposed for asymmetric heat exchangers, *Flow, Turbulence and Combustion* 89(1) (2012) 149–169. doi:10.1007/s10494-012-9387-y.
- [9] A. Colleoni, A. Toutant, G. Olalde, J.-M. Foucaut, Optimization of winglet vortex generators combined with riblets for wall/fluid heat exchange enhancement, *Applied Thermal Engineering* 50 (2013) 1092–1100. doi:10.1016/j.applthermaleng.2012.08.036.
- [10] W. Cai, J. Zhang, X. Zhang, Y. Wang, X. Qi, Enhancement of CO<sub>2</sub> absorption under Taylor flow in the presence of fine particles, *Fluid Dynamics and Transport Phenomena, Chinese Journal of Chemical Engineering* 21(2) (2013) 135–143. doi:10.1016/S1004-9541(13)60451-6.

- [11] N. J. R. Kraakman, J. Rocha-Rios, M. C. M. van Loosdrecht, Review of mass transfer aspects for biological gas treatment, *Applied Microbiology Biotechnology* 91 (2011) 873–886. doi: 10.1007/s00253-011-3365-5.
- [12] D. Taherdazeh, C. Picioreanu, H. van Harald, Mass transfer enhancement in moving biofilm structures, *Biophysical Journal* 102 (2012) 1483–1492. doi: 10.1016/j.bpj.2012.02.033.
- [13] G. P. Aravind, M. Deepu, Numerical study on convective mass transfer enhancement by lateral sweep vortex generators, *International Journal of Heat and Mass Transfer* 115 (2017) 809–825. doi: 10.1016/j.ijheatmasstransfer.2017.07.104.
- [14] A. Al Mers, A. Azzabakh, A. Mimet, H. El Kalkha, Optimal design study of cylindrical finned reactor for solar adsorption cooling machine working with activated carbonammonia pair, *Applied Thermal Engineering* 26 (2006) 1866–1875. doi: 10.1016/j.applthermaleng.2006.01.021.
- [15] J. Saïen, H. Bamdadi, S. Daliri, Liquid–liquid extraction intensification with magnetite nanofluid single drops under oscillating magnetic field, *Journal of Industrial and Engineering Chemistry* 21 (2015) 1152–1159. doi: 10.1016/j.jiec.2014.05.028.
- [16] T. Elperin, A. Fominykh, Mass transfer during solute extraction from a fluid sphere with internal circulation in the presence of alternating electric field, *Chemical Engineering and Processing* 45 (2006) 578–585. doi: 10.1016/j.cep.2006.01.002.
- [17] M. Kordac, V. Linek, Mechanism of enhanced gas absorption in presence of fine solid particles. effect of molecular diffusivity on mass transfer coefficient in stirred cell, *Chemical Engineering Science* 61 (2006) 7125–7132. doi: 10.1016/j.ces.2006.06.025.
- [18] S.-S. Ashrafmansouri, M. N. Esfahany, Mass transfer in nanofluids: A review, *International Journal of Thermal Sciences* 82 (2014) 84–99. doi: 10.1016/j.ijthermalsci.2014.03.017.
- [19] V. Bianco, O. Manca, S. Nardini, K. Vafai, *Heat Transfer Enhancement with Nanofluids*, Taylor & Francis Group, Boca Raton, FL, 2015, ISBN:978-1-4822-5402-0.
- [20] H. V. Moradi, J. M. Floryan, On the mixing enhancement in annular flows, *Physics of Fluids* 29, 024106. doi: 10.1063/1.4976325.
- [21] T. Winnemöller, M. Meinke, W. Schröder, Comparison of the mixing efficiency of different injector configurations, *Computers & Fluids* 117 (2015) 262–272. doi: 10.1016/j.compfluid.2015.05.017.
- [22] J. Aubin, M. Ferrando, V. Jiricny, Current methods for characterising mixing and flow in microchannels, *Chemical Engineering Science* 65(6) (2010) 2065–2093. doi: 10.1016/j.ces.2009.12.001.
- [23] G. J. Nathan, J. Mi, Z. T. Alwahabi, G. J. R. Newbold, D. S. Nobes, Impacts of a jets exit flow pattern on mixing and combustion performance, *Progress in Energy and Combustion Science* 32 (2006) 496–538. doi: 10.1016/j.pecs.2006.07.002.
- [24] A. Bejan, A study of entropy generation in fundamental convective heat transfer, *Transactions of the ASME* 101(4) (1979) 718–725. doi: 10.1115/1.3451063.
- [25] G. P. Narayan, J. H. V. Lienhard, S. M. Zubair, Entropy generation minimization of combined heat and mass transfer devices, *International Journal of Thermal Sciences* 49(10) (2010) 2057–2066. doi: 10.1016/j.ijthermalsci.2010.04.024.
- [26] C. Lou, Z. Zhang, Experimental and numerical analysis of radiative entropy generation in industrial and boiler furnaces, *Journal of Quantitative Spectroscopy & Radiative Transfer* 232 (2019) 27–34. doi: 10.1016/j.jqsrt.2019.04.039.
- [27] F. Bouras, M. E. H. Attia, F. Khaldi, Entropy generation optimization in internal combustion engine, *Environmental Processes* 2 (Suppl 1):233 (2015) 233–242. doi: 10.1007/s40710-015-0102-6.
- [28] M. Bidi, M. R. H. Nobari, M. S. Avval, A numerical evaluation of combustion in porous media by EGM (entropy generation minimization), *Energy* 35(8) (2010) 3483–3500. doi: 10.1016/j.energy.2010.04.053.
- [29] S. Qayyum, T. Hayat, M. I. Khan, M. Khan, A. Alsaedi, Optimization of entropy generation and dissipative nonlinear radiative Von Karman’s swirling flow with Soret and Dufour effects, *Journal of Molecular Liquids* 262 (2018) 261–274. doi: 10.1016/j.molliq.2018.04.010.
- [30] M. Bouabid, N. Hidouri, M. Magherbi, A. Ben Brahim, Heat and mass transfer for Hartmann and Dufour’s effects on irreversibilities at double-diffusive natural convection in a square cavity, *Journal of Advanced Chemical Engineering* 7:2. doi: 10.4172/2090-4568.1000180.
- [31] S. Mahmud, S. H. Tasnim, M. A. H. Mamun, Thermodynamic analysis of mixed convection in a channel with transverse hydro-magnetic effect, *International Journal of Thermal Sciences* 42 (2003) 731–740. doi: 10.1016/S1290-0729(03)00040-1.
- [32] A. Bejan, Entropy generation minimization: the new thermodynamics of finite-sized devices and finite-time processes, *Journal of Applied Physics* 79(3) (1996) 1191–1218. doi: 10.1063/1.362674.
- [33] A. Bejan, *Entropy generation minimization*, CRC Press, 1996, ISBN: 0-8493-9651-4.
- [34] T. A. Jankowski, Minimizing entropy generation in internal flows by adjusting the shape of the cross-section, *International Journal of Heat and Mass Transfer* 52 (2009) 3439–3445. doi: 10.1016/j.ijheatmasstransfer.2009.03.016.
- [35] Q. Li, X. Yuan, P. Neveu, G. Flamant, L. Luo, A novel optimization approach to convective heat transfer enhancement for solar receivers, *Chemical Engineering Science* 116 (2014) 806–816. doi: 10.1016/j.ces.2014.05.051.
- [36] S. Jia, C. Zhang, X. Yuan, K.-T. Yu, An optimization approach to find the thermodynamic limit on convective mass transfer enhancement for a given viscous dissipation, *Chemical Engineering Science* 146 (2016) 26–34. doi: 10.1016/j.ces.2016.01.059.
- [37] X. Cao, S. Jia, Y. Luo, X. Yuan, Z. Qi, K.-T. Yu, Multi-objective optimization method for enhancing chemical reaction process, *Chemical Engineering Science* 195 (2019) 494–506. doi: 10.1016/j.ces.2018.09.048.
- [38] X. Cao, S. Jia, J.-M. Avellaneda, Y. Luo, X. Yuan, G. Flamant, K.-T. Yu, An optimization method to find the thermodynamic limit on enhancement of solar thermal decomposition of methane, *International Journal of Hydrogen Energy* 44(31) (2019) 16164–16175. doi: 10.1016/j.ijhydene.2019.04.261.
- [39] S. Jia, X. Qian, Y. Luo, X. Yuan, K.-T. Yu, A criterion beyond conservation equations for complex transport process modeling a case of Rayleigh-Bénard convection, *Chemical Engineering Science* 128 (2018) 44–55. doi: 10.1016/j.ces.2018.02.017.
- [40] J. M. Avellaneda, S. Jia, P. Neveu, F. Bataille, X. Yuan, G. Flamant, Similarities between heat and mass transfer enhancement in convective flow, using variational optimization technique, *International Heat Transfer Conference* 16, 2018. 10-15 August, Beijing, China. (2018) 2715–2722. doi: 10.1615/IHTC16.cov.021341.
- [41] C. G. Carrington, Z. F. Sun, Second law analysis of combined heat and mass transfer phenomena, *International Journal of Heat and Mass Transfer* 34(11) (1991) 2767–2773. doi: 10.1016/0017-9310(91)90235-7.
- [42] S. S. Rao, *Engineering Optimization*, John Wiley & Sons, Hobo-

ken, New Jersey, 2009, ISBN: 978-0-470-18352-6.

- 1015 [43] I. M. Gelfand, S. V. Fomin, *Calculus of variations*, Prentice-Hall, Englewood Cliffs, New Jersey, 1963, ISBN: 978-0-486-41448-5.
- [44] J. L. Troutman, *Variational calculus and optimal control*, Springer, 1996, ISBN: 978-1-4612-6887-1. doi:10.1007/978-1-4612-0737-5.
- 1020 [45] F. Zonta, C. Marchioli, A. Soldati, Modulation of turbulence in forced convection by temperature-dependent viscosity, *Journal of Fluid Mechanics* 691 (2012) 150–174. doi:10.1017/jfm.2012.67.

1025 **Nomenclature**

$\bar{c}$	Total molar concentration (molarity) [ $mol.m^{-3}$ ]
$\bar{M}_i$	Molar mass of chemical species number $i$ [ $kg.mol^{-1}$ ]
$\bar{R}$	Ideal gas constant (molar) [ $J.K^{-1}.mol^{-1}$ ]
1030 $\mathbf{F}$	Volume force vector by unit of volume [ $N.m^{-3}$ ]
$\mathbf{V}$	Velocity vector [ $m.s^{-1}$ ]
$\dot{m}_1$	Mass production time rate by unit of surface of the chemical minor species (mass flux density) [ $kg.m^{-2}.s^{-1}$ ]
1035 $\dot{S}_{gen}'''$	Local entropy generation rate [ $W.K^{-1}.m^{-3}$ ] (eq. 5 or 7)
$\dot{S}_{gen,d}$	Entropy generation rate from the diffusion process (heat conduction or mass diffusion) in the channel [ $W.K^{-1}$ ]
1040 $\dot{S}_{gen,f}$	Viscous friction entropy generation rate in the channel [ $W.K^{-1}$ ]
$\dot{S}_{gen}$	Total entropy generation rate in the channel [ $W.K^{-1}$ ]
$\lambda_i$	Lagrange multiplier
1045 $\mu$	Dynamic viscosity [ $Pa.s$ ]
$\phi$	Viscous dissipation function [ $W.m^{-3}$ ] (eq. 6)
$\Phi_{tot}$	Total viscous dissipation in the channel [ $W$ ]
$\rho$	Density [ $kg.m^{-3}$ ]
$C_p$	Thermal capacity [ $J.kg^{-1}.K^{-1}$ ]
1050 $D$	Diffusion coefficient [ $m^2.s^{-1}$ ]
$I_s$	Improvement factor (Eq. 19)
$J, J^*$	Objective functional and Lagrangian criterion respectively [ $W.K^{-1}$ ]
$k$	Thermal conductivity [ $W.m^{-1}.K^{-1}$ ]
1055 $P$	Pressure [ $Pa$ ]
$q''$	Heat flux density [ $W.m^{-2}$ ]
$Re$	Reynolds number (based upon the channel height)
$T_{in}$	Inlet temperature [ $K$ ]

1060 $u, v$	Longitudinal and normal components of the velocity [ $m.s^{-1}$ ]
$U_{in}$	Inlet (longitudinal) velocity [ $m.s^{-1}$ ]
$w_i$	Mass fraction of chemical species number $i$ [ $kg.kg^{-1}$ ]
1065 $w_{1,in}$	Inlet mass fraction of chemical minor species [ $kg.kg^{-1}$ ]
$W_{\Phi}$	Weighting factor in objective functional and Lagrangian criterion [ $K^{-1}$ ]
$x, y$	Longitudinal and normal coordinates [ $m$ ]
1070 $T$	Temperature [ $K$ ]